Segregation and flow during the solidification of alloys

A.O.P. Chiareli, Herbert E. Huppert, M. Grae Worster

*Institute of Theoretical Geophysics, Department of Applied Mathematics and Theoretical Physics, Silver Street,
Cambridge CB3 9EW, UK*

Abstract

The crystallization of a binary alloy from a cooled boundary is analysed and the structure of the resulting solid product examined. The analysis includes effects due to differences in densities between solid and liquid phases and due to a non-zero segregation coefficient of the alloy. We determine the general conditions under which the solidification takes place either at a planar interface or throughout a mushy layer of solid dendrites bathed in interstitial fluid. We are able to make significant analytical progress by finding appropriate similarity solutions of the governing differential equations, and then simplifying these solutions in the asymptotic limit of practical interest wherein the compositional diffusivity is very much less than the thermal diffusivity. Thereby we determine a simple criterion that distinguishes between the solidification at a planar front being controlled mainly by the transport of the rejected component away from the phase boundary rather than by the associated thermal transports. We also calculate the solid fraction and the degree of micro-segregation in the mushy layer. In addition, the density difference between the liquid and solid phases is shown to induce a flow of the liquid phase during solidification, which causes macro-segregation of the resulting solid product.

1. Introduction

As a multi-component fluid cools and solidifies, the interface between fluid and solid is either planar or distorted within a comparatively broad zone in which solid crystals are bathed in liquid. Such a zone is known as a mushy layer. Investigation of the evolution of mushy layers cannot readily be carried out by the detailed study of the growth of individual crystals. Instead, it is more productive to use the approach of continuum mechanics whereby at each point in the mushy layer suitable averages are taken over a volume that contains many crystals to determine local values of the temperature, solute concentration and (volume) solid fraction ϕ.

Our understanding of the dynamics of solidification has been greatly enhanced by the exact analytical solution of simple models. The similarity solution for growth of a planar crystal front in a pure melt, for example, is now part of the established literature of problems in heat transfer [1] and was extended by Rubinstein [2] to simple binary alloys. Theoretical models describing the evolution of mushy layers have advanced significantly over the last decade (see ref. [3] for a review) guided to a large extent by concurrent laboratory experiments [4].

Encouraged by the excellent agreement between the predictions of the equations for a stagnant mushy layer presented by Worster [5] and the results of laboratory experiments, this paper develops the previous approach to new situations. We examine effects due to either the flow induced when the solid and liquid have different densities or to a non-zero segregation coefficient of the alloy, whereby a proportion of both components in the liquid phase are taken into the solid. Some of the effects have been included previously in numerical simulations of solidifying systems without the important consequences being specifically identified [6]. By our analytical approach, we are able to elucidate the roles of the segregation coefficient and the density ratio individually. One of the aims of the paper is to examine spatial variations on both a small and large scale, or the micro- and macro-segregation that can occur during solidification of a binary melt.

We are able to make significant progress in determining simple analytical expressions by exploiting the practical asymptotic limit of small compositional diffusion relative to thermal diffusion. Mathematically, this is achieved by letting ϵ_ℓ, $\epsilon_s \rightarrow 0$, where $\epsilon_{\ell,s} = (D/\kappa_{\ell,s})^{1/2}$, D is the

solutal diffusivity in the liquid phase, and κ_s and κ_ℓ are the thermal diffusivities of the solid and the liquid phases, respectively.

The plan of the paper is as follows. Solidification at a flat interface is analysed in section 2. Similarity solutions are obtained and a completely general expression is found for the rate of solidification. Asymptotic approximations are used to determine simple expressions for the external conditions under which evolution of the interface is controlled mainly by the diffusion of solute, rather than by the diffusion of heat. The consequences for heat and mass transfer of the flow caused by either expansion or shrinkage during solidification are identified and the segregation caused by such flow is calculated. The conditions under which the interface can remain planar are presented in section 3, and thus the conditions are obtained under which mushy layers can be expected to form. Equations governing the evolution of mushy layers are presented in section 4. These are used to determine ordinary differential equations describing similarity solutions for the solidification of an alloy from a cooled, plane boundary of fixed temperature. The model is used to predict the consequences of the flow within the interstices of the mushy layer on
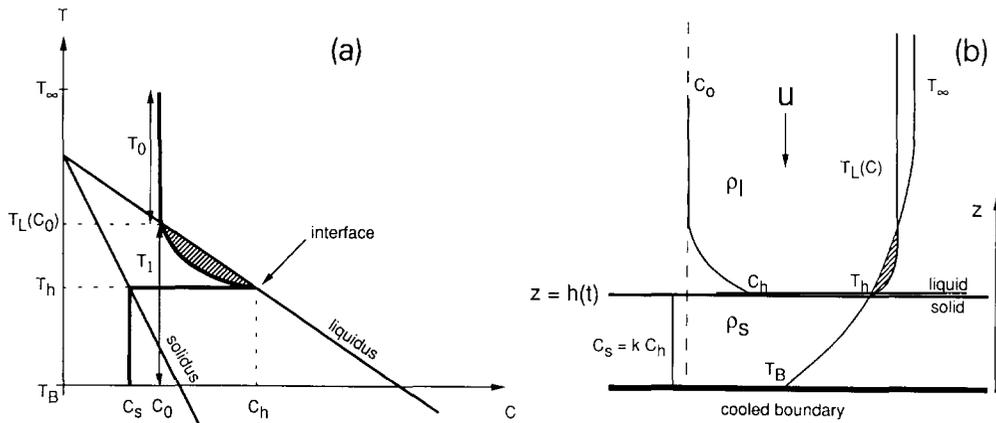

Fig. 1. (a) Part of the phase diagram for a binary alloy, which shows the solidus and liquidus curves for temperatures above the eutectic temperature. The thick solid line shows the trajectory of the temperature and composition during solidification from a planar boundary. (b) Schematic diagram of solidification from a plane wall when the solid–liquid interface remains flat. The velocity field u is driven by differences in density between the solid and liquid phases. In the case $\rho_s > \rho_\ell$, the velocity field is towards the solid–liquid interface, as illustrated. The hatched region in each figure shows a region of constitutional supercooling in which the temperature just ahead of the interface is lower than the local liquidus temperature.

the overall growth rate of the layer and on the distribution of solid within it. The latter is particularly important in determining the permeability of the layer. Further, the redistribution of solute is calculated, which gives an indication of the level of macro-segregation to be expected in a fully solidified system. The value of the segregation coefficient has a primary effect on the microscopic segregation of the alloy, and we determine how this affects the overall dynamics of the mushy layer.

2. Planar solidification front

2.1. The governing equations

In this section, we present analytical results for solidification at a planar front of a two-component fluid having the typical phase diagram shown in Fig. 1a. A sketch of the problem under consideration is given in Fig. 1b. The region $z > 0$ is initially filled with fluid of uniform density ρ_ℓ and composition $C = C_0$ at temperature T_∞, which exceeds the initial liquidus temperature $T_L(C_0)$. The binary alloy is solidified from a flat cooled boundary at $z = 0$, which is held at a fixed temperature $T_B < T_L(C_0)$. Solid forms at the boundary and is separated from the melt by a planar interface at $z = h(t)$. The value of the temperature and concentration of the liquid at the interface are denoted by T_h and C_h, respectively. The solid has uniform density ρ_s which in general is different from the liquid density ρ_ℓ. We specifically include and investigate the flow of melt caused by such a density difference, where the flow is towards the solid–melt interface in the case of contraction of the solid ($\rho_s > \rho_\ell$) or away from the interface in the case of expansion ($\rho_s < \rho_\ell$).

We investigate situations in which gravity has no influence on the motion of the fluid. Such would be the case, for example, when the melt is cooled from below and heavy solute is rejected during solidification, so that both the temperature and the compositional fields are stable to buoyancy driven convection.

The solutal diffusion coefficient in the solid is negligible in comparison with that in the liquid, so the solid concentration established at the crystal–liquid interface is frozen in. The differential equations governing the temperature field $T(z, t)$ and the concentration of the liquid phase $C(z, t)$ are the advection–diffusion equations

$$T_t = \kappa_s T_{zz} \qquad (z < h(t)), \qquad (2.1)$$

$$T_t + uT_z = \kappa_\ell T_{zz} \qquad (z > h(t)), \qquad (2.2)$$

$$C_t + uC_z = DC_{zz} \qquad (z > h(t)). \qquad (2.3)$$

The physical parameters are the thermal diffusivities κ_s and κ_ℓ, and the solute diffusivity D, which are assumed constant in each phase.

In the absence of any driving forces, the velocity of the melt u is determined solely by conservation of mass at the solid–liquid interface, which requires that

$$u = (1 - r) \, dh/dt, \qquad (2.4)$$

where the ratio of densities $r = \rho_s/\rho_\ell$ is such that $r > 1$ corresponds to contraction and $r < 1$ to expansion.

The above equations are subject to the following boundary and initial conditions

$$T = T_B \qquad (z = 0), \qquad (2.5a)$$

$$T = T_h, \quad C = C_h, \qquad (z = h(t)), \qquad (2.5b,c)$$

and

$$T \rightarrow T_\infty, \quad C \rightarrow C_0 \qquad (z \rightarrow \infty \text{ or } t \rightarrow 0). \quad (2.6a,b)$$

There are also two flux conditions to be applied at the unknown position of the interface $h(t)$. Conservation of heat requires that the latent heat of solidification be diffused away from the interface so that

$$\mathscr{L} \, dh/dt = K_s T_z \mid_{z-h_-} - K_\ell T_z \mid_{z-h_+}, \qquad (2.7)$$

where $\mathscr{L}$ is the latent heat per unit volume of solid, $K = c\kappa$ is the thermal conductivity, and c is the heat capacity per unit volume. Throughout this paper, material properties will be written in terms of values per unit volume, so that variations in $r = \rho_s/\rho_\ell$ affect only the velocity field and not the material properties. Conservation of solute requires that

$$r(1 - k)C_h \, dh/dt = -DC_z \mid_{z=h_+}. \qquad (2.8)$$

The solidus relation $C_s = kC_h$ and the definition of u given by Eq. (2.4) were used to obtain the expression above, where k is the segregation coefficient and C_s is the concentration in the solid at the interface. Finally, we make the assumption that the interface is at thermodynamic equilibrium, so that the temperature and concentration at the interface are related by the liquidus

$$T(h, t) = -mC(h_+, t), \qquad (2.9)$$

where the liquidus slope m is taken to be constant.

The system of partial differential equations (2.1)–(2.4) admits a similarity solution with variable

$$\eta = z/2\sqrt{Dt}, \qquad (2.10)$$

in which the interface has position

$$h(t) = 2\lambda\sqrt{Dt}, \qquad (2.11)$$

where the constant λ is to be determined. These similarity solutions are such that, with the given boundary conditions, solutions of the full partial-differential system will tend to the similarity solution for arbitrary, smooth initial conditions [7,8]. We scale $h(t)$ in terms of the compositional diffusivity, rather than the thermal diffusivity, since the rate of solidification of an alloy at a planar interface is generally controlled by the relatively slower diffusion of solute [9]. The governing equations reduce to ordinary differential equations in the similarity variable, and can be integrated to give

$$T = T_B + (T_h - T_B)\frac{\mathrm{erf}(\epsilon_s \eta)}{\mathrm{erf}(\epsilon_s \lambda)} \quad \eta > \lambda \ (\text{solid}),$$
$$(2.12a)$$

$$T = T_\infty + (T_h - T_\infty)\frac{\mathrm{erfc}(\epsilon_\ell \gamma)}{\mathrm{erfc}(\epsilon_\ell \lambda r)} \quad \eta < \lambda \ (\text{liquid}),$$
$$(2.12b)$$

$$C = C_0 + (C_h - C_0)\frac{\mathrm{erfc}(\gamma)}{\mathrm{erfc}(\lambda r)} \quad \eta < \lambda \ (\text{liquid}),$$
$$(2.12c)$$

where

$$\gamma = (r - 1)\lambda + \eta, \qquad (2.13)$$

and $\epsilon_{\ell,s} = (D/\kappa_{\ell,s})^{1/2}$.

Relationships between the three unknowns λ, C_h, and T_h are determined by the three interfacial conditions (2.7)–(2.9). In particular, we determine the interfacial position λ as the root of

$$mC_0\left(\frac{(1-k)\,F(r\lambda)}{1-(1-k)\,F(r\lambda)}\right)\left(\frac{1}{G(\epsilon_s\lambda)} + \frac{r\beta}{F(\epsilon_\ell r\lambda)}\right)$$
$$= \frac{T_1}{G(\epsilon_s\lambda)} - \frac{r\beta T_0}{F(\epsilon_\ell r\lambda)} - \frac{\mathscr{L}}{c_s}, \qquad (2.14)$$

where $\beta = c_\ell/c_s$ is the ratio of specific heats, which we keep fixed during the analysis, and where

$$F(x) = \sqrt{\pi}\,x \exp(x^2)\,\mathrm{erfc}(x) \sim \sqrt{\pi}\,x \quad (x \to 0),$$
$$(2.15a)$$

$$G(x) = \sqrt{\pi}\,x \exp(x^2)\,\mathrm{erf}(x) \sim 2x^2 \quad (x \to 0).$$
$$(2.15b)$$

The driving temperature differences

$$T_0 = T_\infty - T_L(C_0), \quad T_1 = T_L(C_0) - T_B,$$
$$(2.16a,b)$$

are illustrated in Fig. 1a.

Eq. (2.14) represents the most general eigenvalue relationship for λ. Several special cases of this result have appeared previously. For example, the case $r = 1$, $C_0 = 0$, which applies to the solidification of a pure melt without contraction, is the classical Stefan problem solved by Neumann in the 1860's [1]. Solidification of a pure melt with contraction ($C_0 = 0$, $r \neq 1$) is described in a recent text by Alexiades and Solomon [10], while solutions for a binary melt without contraction ($C_0 \neq 0$, $r = 1$) have been given by Rubinstein [2] and by Huppert and Worster [9]. In the general relationship (2.14) we have included effects due both to convection and to having a non-zero segregation coefficient k in a binary melt.

2.2. Compositional versus thermal control

The relationship (2.14) is a complicated, transcendental equation for λ, which may not have a solution for certain parameters. For example, no solution exists for growth into a pure, hyper-

cooled melt; $C_0 = 0$, $T_1 = 0$, $T_0 < -\mathscr{L}/rc_\ell$. In cases when a solution does exist, the equation can be solved numerically given specific values of the external parameters. However, the equation has a simpler form in the asymptotic limit ϵ_ℓ, $\epsilon_s \to 0$, which allows considerable analytical progress to be made and fresh physical insight to be gained. This is a useful, practical limit to consider since the diffusivity of heat is typically much greater than the diffusivity of solute.

Under the assumption that λ remains finite in the limit ϵ_s, $\epsilon_\ell \to 0$, with all other parameters fixed, $G(\epsilon_s \lambda) \ll F(\epsilon_\ell r \lambda)$ and Eq. (2.14) reduces to

$$T_1 = \frac{mC_0(1-k) \, F(r\lambda)}{1 - (1-k) \, F(r\lambda)}, \qquad (2.17)$$

which can be rearranged to give

$$F(r\lambda) = \frac{1}{1-k}\left(1 + \frac{mC_0}{T_1}\right)^{-1}. \qquad (2.18)$$

Since $F(x)$ increases monotonically from 0 to 1 as x increases from 0 to ∞, (2.18) always has a unique solution if

$$0 < T_1 < (1-k)mC_0/k. \qquad (2.19)$$

This condition can be expressed in terms of external parameters as

$$-mC_0/k < T_B < -mC_0. \qquad (2.20)$$

Condition (2.20) is one of the central results of this study and indicates that there is always a solution of (2.18) if the temperature of the base is between the solidus and liquidus temperatures evaluated at the far-field composition. The existence of such a solution confirms that, in this situation, the scaling suggested by (2.11) is appropriate and that the solidification at a planar interface is indeed controlled by the diffusion of solute ahead of the interface.

Conversely, if the temperature of the cold base T_B is less than the solidus temperature $-mC_0/k$, then either a thermal diffusivity should be used in (2.11) or it should be appreciated that λ is of order ϵ^{-1}. In this regime, the transport of solute is no longer the rate-controlling process and the interface advances much more rapidly, at a rate determined by thermal diffusion. If we take the

limit ϵ_s, $\epsilon_\ell \to 0$ with $\mu = \epsilon_\ell \lambda = O(1)$, then the general expression (2.14) becomes

$$\frac{-mC_0/k - T_B}{G(\epsilon_s \mu / \epsilon_\ell)} - \beta r \frac{T_\infty + mC_0/k}{F(r\mu)} = \frac{\mathscr{L}}{c_s}. \qquad (2.21)$$

Eq. (2.21) is similar to that obtained in the classical Stefan problem [1] and shows that, in this thermally controlled regime, the binary alloy solidifies at the same rate as a pure melt of freezing temperature $T_m = -mC_0/k$, which is the solidus temperature of the original melt. In Fig. 2a, the dimensionless growth rate λ calculated from the full expression (2.14) is plotted as a function of T_B. Superimposed on the same graph are the solutions of the asymptotic expressions (2.18) and (2.21), which are seen to give very good approximations in the regimes corresponding to compositional control and thermal control respectively.

The preceding discussion indicates that the value of the segregation coefficient k affects the rate of solidification significantly because its value determines how much solute is rejected at the interface upon solidification. It is straightforward to deduce that the system is compositionally controlled in the extreme case $k = 0$ (total rejection of solute) and thermally controlled in the opposite extreme $k = 1$ (total incorporation of solute). It is of interest to know at what value of k the system changes from being compositionally controlled to being thermally controlled.

From (2.20) we obtain the asymptotic result that for values of $k < -mC_0/T_B$ the system is compositionally controlled, whereas if this condition is violated, the system is thermally controlled. For the parameter values in Table 1, we bring this result to a plot of numerical solutions in Fig. 2b. We see that the asymptotic result for k we have just found, which is marked by the dashed line, corresponds to an inflection point in the full solution. Results are shown for three different values of the density ratio r. The growth rate depends significantly on this parameter. In particular, it appears that when r is very small, corresponding to large expansion, the rate of solidification is no longer controlled by diffusion of solute.

2.3. Convective effects due to expansion or contraction

Contraction or expansion during solidification induces the melt to flow, which affects the solidification process in a number of ways. The transport of heat and solute are both altered by the velocity field u which thus affects the rate of solidification as well as the composition in the final solid. In the case of contraction ($r > 1$), for
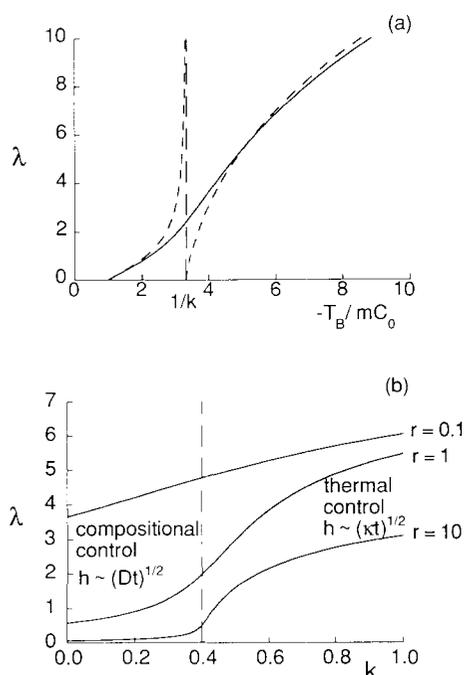
Table 1

Parameter values used in our calculations except where otherwise stated; these are typical of a laboratory experiment in which a solution of sodium nitrate, $NaNO_3$, is cooled from below

L	73.6 cal cm^{-3}
D	1×10^{-5} cm^2 s^{-1}
K_s	5.3×10^{-3} cal g^{-1} s^{-1} °C^{-1}
K_ℓ	1.3×10^{-3} cal g^{-1} s^{-1} °C^{-1}
ρ_s	0.92 g cm^{-3}
ρ_ℓ	1.25 g cm^{-3}
m	0.4°C wt%$^{-1}$
c_s	0.44 cal cm^{-3} °C^{-1}
c_ℓ	1.25 cal cm^{-3} °C^{-1}
T_∞	20°C
T_B	-14°C
C_0	14 wt%

example, the flow in the melt is towards the interface and compresses both the thermal and compositional boundary layers, enhancing the transport of heat towards the interface and the transport of solute away from the interface. The former inhibits an increase in the rate of solidification while the latter promotes it.

Solving (2.14) for λ as a function of r, we obtain the numerical plots presented in Fig. 3 which illustrates how r affects the growth rate of the interface. As the density ratio increases, the

Fig. 2. (a) The growth-rate parameter λ as a function of the temperature of the cold base T_B, normalized with the liquidus temperature $-mC_0$. The rate of solidification is controlled by diffusion of solute ahead of the interface when the base temperature is greater than the solidus temperature $-mC_0/k$. The graph is plotted for a value of the segregation coefficient $k = 0.3$. When the base is colder than the solidus temperature, the solid grows as if from a pure melt of freezing temperature equal to the solidus temperature. Shown with dashed lines are asymptotic results in the limit of small solutal diffusivity relative to the thermal diffusivity. (b) λ plotted as a function of k for different values of the density ratio r. The dashed line shows the value of k determined by asymptotic analysis in the limit $\epsilon_{\ell s} \rightarrow 0$ for which the system changes from being compositionally controlled to being thermally controlled. The parameters used for both plots are listed in Table 1.
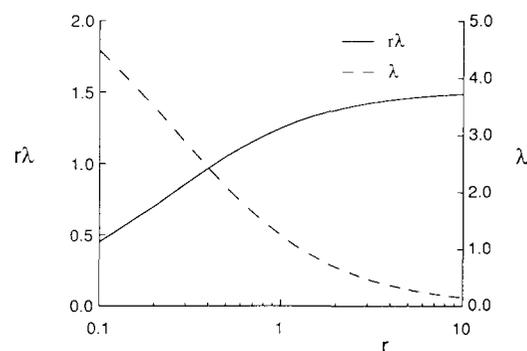

Fig. 3. Superposed in the same plot are the rate of accretion of mass to the solid, proportional to $r\lambda$, and the growth rate of the interface as functions of r. As r increases, the rate of mass accretion increases due to the enhanced mass transport towards the solid, but the interface grows more slowly because the solidified melt occupies less space than it did in the liquid state. The parameters used to calculate these curves are listed in Table 1, with $k = 0.3$.

rate of mass accretion to the solid, which is proportional to λr, increases as shown in Fig. 3. However, this mass occupies less space than it did in the liquid state, so the interface actually advances less rapidly with increasing density ratio r, as illustrated in the superposed plot also in Fig. 3.

2.4. Segregation

An important technological question is how to predict and thence control the final solid composition C_s. From Eq. (2.8), the concentration in the liquid at the interface C_h can be determined and this, together with the solidus relation, gives the following expression for the composition in the solid:

$$C_s = kC_0 \left(\frac{(1-k)\,F(r\lambda)}{1-(1-k)\,F(r\lambda)} + 1 \right). \qquad (2.22)$$

Useful approximate solutions of (2.22) can be obtained in the asymptotic regimes corresponding to compositional or thermal control of the interface. When the growth is compositionally controlled, $F(r\lambda)$ is given by Eq. (2.18), which can be used in (2.22) to show that

$$C_s \sim -kT_B/m. \qquad (2.23)$$

Since the thickness of solid grown is much less than the width of the thermal boundary layer in this regime, the temperature of the interface is almost equal to the temperature of the cold boundary T_B. Therefore, the concentration in the liquid at the interface is $-T_B/m$, according to the liquidus relationship, and (2.23) follows from the solidus relationship. On the other hand, when $\lambda \gg 1$, Eq. (2.22) is approximated by

$$C_s \sim C_0. \qquad (2.24)$$

In this limit, the concentration of the solid is almost equal to the initial concentration of the liquid; there is little segregation, which explains why compositional control is replaced by thermal control.

These asymptotic results are shown in Fig. 4 to give good predictions for moderate values of the density ratio r. When r is large, contraction causes the solid–liquid interface to advance even less rapidly than the isotherms and therefore the
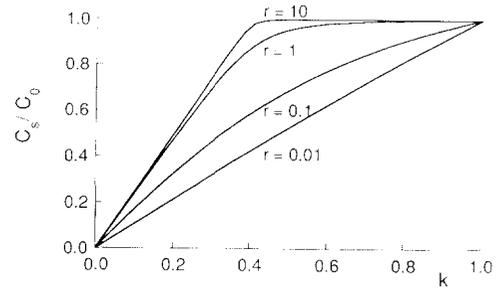

Fig. 4. Normalized concentration in the solid C_s/C_0 as a function of the segregation coefficient k for different values of the density ratio r. The curves were calculated using the parameters in Table 1. When the system is compositionally controlled ($k < 0.4$), the solid composition increases almost linearly with k. When the system is thermally controlled ($k > 0.4$), the composition of the solid is almost independent of the segregation coefficient k and is approximately equal to the initial composition of the melt. This general behaviour does not apply for very small values of the density ratio r, when growth is less inhibited by transport of solute and the composition of the solid varies linearly with k as shown for the whole range $0 < k < 1$.

full solution follows the asymptotic solutions (2.23) and (2.24) more closely.

Segregation is more sensitive to the value of the density ratio r in the case of expansion. Indeed, as $r \to 0$,

$$C_s \to kC_0 \qquad (2.25)$$

in both compositionally and thermally controlled regimes, a result which has quite a different character from when $r = O(1)$, as seen in Fig. 4. The flow caused by expansion transports solute away from the interface, whose growth is therefore less dependent on the rate of solutal diffusion.

3. Instability of a planar interface

Solidification at a growing interface is said to undergo constitutional supercooling if the temperature and composition fields in the fluid lie below the local liquidus (see Fig. 1). This would imply, inconsistently, that the melt is partially solid. Mathematically, the condition for this to occur is that

$$T_z \mid_{h_-} < -mC_z \mid_{h_-}, \qquad (3.1)$$

(as first derived by Rutter and Chalmers [11], and reviewed by Sekerka [12]). A quantitative dynamical calculation indicates that, in the absence of the Gibbs–Thompson effect, the interface is exponentially unstable in time to infinitesimal disturbances, and is said to be morphologically unstable (as first derived in Mullins and Sekerka [13]), if

$$K_s T_z \mid_{h_-} + K_\ell T_z \mid_{h_+} < -m(K_s + K_\ell)C_z \mid_{h_+}.$$

$$(3.2)$$

An alternative expression is obtained by substituting (2.7) into (3.2) to indicate that morphological instability sets in if

$$T_z \mid_{h_+} < \left[-m(K_s + K_\ell)C_z \mid_{h_+} - \mathscr{L}\dot{h} \right]/2K_\ell.$$

$$(3.3)$$

where $\dot{h} = dh/dt$. Eq. (3.2) approximates to (3.1) if $K_s \ll K_\ell$. We proceed on the assumption that effects due to shrinkage do not alter this internal criterion for instability (a discussion of this problem is given in ref. [14]). In terms of the similarity solution we obtained in section 2, we can determine the conditions for which either (3.1) or (3.2) occurs first by differentiating (2.12b) and (2.12c), evaluating the result at $z = h$, and expressing the result as the ratio

$$-mC_z \mid_{h_+}/T_z \mid_{h_+} = \frac{-mC_0(1 - k)\ F(\epsilon_\ell r\lambda)}{\epsilon_\ell^2 (T_\infty - T_h)}.$$

$$(3.4)$$

We can determine the value of T_B for the onset of constitutional supercooling by obtaining the root λ of (3.4), inserting it into (2.14) and solving that equation for T_B. This critical value of T_B is displayed in Fig. 5 as a function of the initial concentration C_0 for a fixed value of T_∞. As illustrated in this figure, a non-zero segregation coefficient considerably widens the window of low concentrations for which the system can be cooled rapidly and still maintain a stable flat solid–liquid interface.

Expression (3.4) takes a simpler form in the limit $\epsilon_\ell \to 0$. In this limit, $F(\epsilon_\ell r\lambda) \sim \pi^{1/2}\epsilon_\ell r\lambda$, so the right-hand side of (3.4) remains finite only if
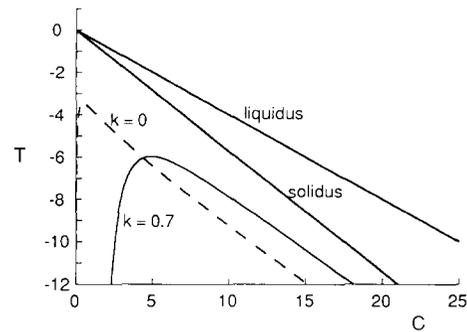

Fig. 5. Phase diagram showing the liquidus curve and the solidus curve for $k = 0.7$. Curves indicating the values of T_B for which supercooling first occurs are also shown. These are for a given fixed far-field temperature, $T_\infty = 20$. The dashed line is for $k = 0$, which shows that only a rather pure melt can be cooled fast without supercooling ocurring. The solid curve is for $k = 0.7$, and there is a window of low concentrations for which the system will keep a stable flat solid–liquid interface even if cooled rapidly. Parameter values for calculating the curves are given in Table 1.

$\lambda = O(\epsilon_\ell)$, or if $mC_0(1 - k) = O(\epsilon_\ell)$ with $\lambda = O(1)$. In the former case, (2.25) indicates that

$$T_1 \sim mC_0(1 - k)\ F(r\lambda),$$

$$(3.5)$$

and, as explained following (2.23),

$$T_h \sim -mC_0 - T_1 = T_B.$$

$$(3.6)$$

The substitution of (3.5) and (3.6) into (3.4) shows that the right-hand side of (3.4) is then approximately $T_1/\epsilon_\ell T_0$. In addition $(\mathscr{L}\dot{h})/(K_\ell T_z \mid_{h_+}) = O(\epsilon_\ell^2)$ and hence can be neglected in (3.3). Thus constitutional supercooling, as expressed by (3.1), occurs if

$$T_1 > \epsilon_\ell T_0,$$

$$(3.7)$$

and morphological instability, as expressed by (3.3), occurs if

$$T_1 > \frac{2K_\ell}{K_s + K_\ell}\epsilon_\ell T_0.$$

$$(3.8)$$

We hence conclude that, except for small values of C_0, if $K_\ell < K_s$ morphological instability occurs first, while if $K_\ell > K_s$ constitutional supercooling occurs before the interface becomes morphologically unstable.

4. Evolution of a mushy layer

In most metallurgical and geophysical processes, as well as in laboratory experiments, the threshold of morphological instability is so far exceeded that the solid–liquid interface develops the form of a mushy layer. Instead of tracing the evolution of this convoluted interface, it is appropriate to treat the mushy layer as a continuum for which averaged equations and physical properties can be used to describe its evolution.

Equations for mushy layers have been presented previously by a number of authors (e.g. Hills, Loper and Roberts [15], Fowler [16], Worster [5]). A derivation of the equations we use here is presented in a recent review by Worster [3].

The governing equations for the mushy layer are given by the local conservation equations for heat and solute, which can be expressed as

$$c_m T_t + c_\ell U \cdot \nabla T = \nabla \cdot (K_m \nabla T) + \mathscr{L}_s \phi_t, \tag{4.1}$$

$$(1 - \phi) C_t + U \cdot \nabla C$$
$$= \nabla \cdot (D_m \nabla C) + rC(1 - k)\phi_t. \tag{4.2}$$

The temperature T and the composition of the interstitial liquid C are assumed to be uniform over length scales typical of the inter-dendritic spacing. The volume fraction of solid dendrites is denoted by ϕ, while U represents the volume flux of inter-dendritic fluid. The physical parameters are as defined in section 2, where the subscript "m" denotes properties of the mushy phase. The terms $\mathscr{L}_s \phi_t$ and $rC\phi_t$ on the right-hand sides of the above conservation equations express the release of latent heat into the mush and of solute into the interstitial fluid respectively.

The thermal properties of the mush are taken to be averages of the properties of the individual phases, so that

$$c_m = \phi c_s + (1 - \phi) c_\ell, \tag{4.3}$$

$$K_m = \phi K_s + (1 - \phi) K_\ell, \tag{4.4a}$$

$$D_m = (1 - \phi) D. \tag{4.4b}$$

Expression (4.3) is exact while expressions (4.4a) and (4.4b) are only approximate because transport properties depend on the internal morphol-

ogy of the two-phase medium [17]. However, its use has been found to lead to theoretical predictions which are in good agreement with experimental results [5,7,18,19], mainly due to alignment of the crystals with the temperature gradient.

The velocity field U must satisfy the continuity equation

$$\nabla \cdot U = (1 - r)\phi_t. \tag{4.6}$$

so that mass is conserved. In the case of a one-dimensional model, this equation is sufficient to determine U. Notice that the divergence of the velocity field is not zero; rather it depends on the rate of change of the solid fraction in a way determined by the density ratio r. For example, in the case of contraction of the solid phase $(r > 1)$, $\nabla \cdot U < 0$. The rate of change of the solid fraction couples Eqs. (4.1), (4.2) and (4.6), and is obtained implicitly through the internal equilibrium condition

$$T = T_l(C) = -mC, \tag{4.7}$$

which says that the temperature is equal to the local liquidus temperature throughout the mushy layer.

The equations above constitute a full set of governing equations for the mushy layer. Three interfacial conditions expressing conservation of heat, solute and mass at the mush-liquid interface can be derived from Eqs. (4.1), (4.2) and (4.6). These can be expressed as

$$\mathscr{L} V_n[\phi] = [K_m n \cdot \nabla T], \tag{4.8a}$$

$$r(1 - k) C_\ell V_n[\phi] = [D_m n \cdot \nabla C], \tag{4.8b}$$

$$(r - 1) V_n[\phi] = [n \cdot U], \tag{4.8c}$$

where [ ] denotes the jump in the enclosed quantity across an interface with normal n moving with normal velocity V_n.

In addition, we impose the condition of marginal equilibrium [3,5]

$$T_z |_{h_-} = -mC_z |_{h_-}. \tag{4.9}$$

There are two boundary conditions to be applied at the bottom of the mushy layer at the cooled boundary. These are

$$T = T_B, \quad n \cdot U = 0 \quad (z = 0). \tag{4.10a,b}$$

The system of partial differential equations described above admits a similarity solution, similar to those found in previous studies [5,19,20], for solidification from a cooled, planar boundary with similarity variable

$$\eta = z/2\sqrt{\kappa_\ell t}\,, \tag{4.11}$$

in which the mush–liquid interface has position

$$h(t) = 2\mu\sqrt{\kappa_\ell t}\,, \tag{4.12}$$

where μ is a constant to be determined as part of the solution. Notice that now the similarity variable is scaled with the thermal diffusivity rather than with the solutal diffusivity. This is because the rate of growth of the mushy layer is controlled principally by the rate of heat transfer, not solute transfer, since the rejected solute is accommodated within the interstices of the mushy layer.

The governing equations reduce to a system of ordinary differential equations in the similarity variable, and can be made dimensionless by scaling temperatures with $\Delta T = T_L(C_0) - T_B$, concentrations with $\Delta C = [T_L(C_0) - T_B]/m$, and the velocity field with $\sqrt{\kappa_\ell/t}$. Upon writing

$$T - T_L(C_0) = \Delta T\, \theta(\eta), \tag{4.13}$$

$$C - C_0 = -\Delta C\, \Theta(\eta), \tag{4.14}$$

$$U = \sqrt{\kappa_\ell/t}\, g(\eta), \tag{4.15}$$

and using the internal equilibrium condition $\Theta = \theta$, the coupled, nonlinear, governing differential equations for temperature, concentration and mass reduce to

$$-c_m\eta\theta' + g\theta' = \tfrac{1}{2}(K_m\theta')' - \mathscr{S}\eta\phi', \tag{4.16}$$

$$(1 - \phi)\eta\theta' - g\theta'$$
$$= -\frac{1}{Le}[(1 - \phi)\theta']' + r(k - 1)(\mathscr{C} - \theta)\eta\phi', \tag{4.17}$$

$$g' = (r - 1)\eta\phi', \tag{4.18}$$

where the dimensionless specific heat and dimensionless thermal conductivity are defined as

$$c_m = (1 - \phi) + (c_s/c_\ell)\phi, \tag{4.19}$$

$$K_m = (1 - \phi) + (K_s/K_\ell)\phi, \tag{4.20}$$

and $\mathscr{S} = \mathscr{L}/(c_\ell\Delta T)$, $Le = \kappa_\ell/D$, and $\mathscr{C} = C_0/\Delta C$. Chiareli and Worster [19] presented these similarity equations with the segregation coefficient k set to zero and showed that they yielded predictions of the solid fraction within the mushy layer that were in good agreement with experimental data.

To obtain the boundary conditions for this system of equations, it is necessary to solve the problem in the liquid region. The appropriate equations there are given by (4.16)–(4.18) with $\phi = 0$, which are readily solved to give

$$g = v, \tag{4.21}$$

$$\theta = \theta_\infty + (\theta_h - \theta_\infty)\frac{\text{erfc}(\eta - v)}{\text{erfc}(\mu - v)}, \tag{4.22}$$

$$\Theta = \Theta_h\frac{\text{erfc}[\sqrt{Le}\,(\eta - v)]}{\text{erfc}[\sqrt{Le}\,(\mu - v)]}, \tag{4.23}$$

where v is a constant, and

$$\theta_\infty = [T_\infty - T_L(C_0)]/\Delta T,$$

$$\theta_h = [T_h - T_L(C_0)]/\Delta T,$$

$$\Theta_h = (C_h - C_0)m/\Delta T.$$

These solutions are similar to those presented in section 2 for the liquid region, but now v is unknown.

The marginal equilibrium condition is expressed in similarity variables by

$$\theta'|_{\text{liquid}} = \Theta'|_{\text{liquid}}, \tag{4.24}$$

and we use this condition together with (4.21)–(4.23) to determine that

$$\Theta_h = (\theta_h - \theta_\infty)\frac{\exp[-(\mu - v)^2]}{\text{erfc}(\mu - v)}$$
$$\times\frac{\text{erfc}[\sqrt{Le}\,(\mu - v)]}{\exp[-\sqrt{Le}\,(\mu - v)^2]}. \tag{4.25}$$

We can deduce from (4.25) that in the limit $Le \to \infty$, $\Theta_h = \theta_h = O(Le^{-1})$. This implies that, to leading order, $\Theta \equiv 0$ in the liquid and therefore that $C_h \sim C_0$ on the liquid side of the interface. Given (4.25), the dimensionless form of (4.8b) in the limit $Le \to \infty$ implies that $[\phi] = 0$ and hence

that $\phi = 0$ at the mush–liquid interface. With the results above, we obtain the following dimensionless boundary conditions for the mushy layer

$$\phi = 0, \quad \theta = 0, \quad g = v, \qquad (4.26a,b,c)$$

$$\frac{d\theta}{d\eta} = \frac{2}{\sqrt{\pi}} \frac{\theta_\infty}{\mathrm{erfc}(\mu - v)} \exp\left[-(\mu - v)^2 \right]$$

$$(\eta = \mu), \qquad (4.26d)$$

and

$$\theta = -1, \quad g = 0 \quad (\eta = 0), \qquad (4.27a,b)$$

where v and μ are to be determined.

The limit $\mathrm{Le} \to \infty$ can be taken in Eq. (4.17) even though the term with the highest derivative is thereby neglected. This does not cause a singular pertubation because the internal equilibrium condition $T = -mC$ couples the thermal and compositional fields in the mushy layer and a derivative of the same order as that neglected in (4.17) is retained in (4.16). This limit simplifies Eq. (4.17), renders the coupled equations (4.16)–(4.18) less stiff and causes the mushy layer to extend to the cold boundary. Otherwise, there is a thin layer of solid between the boundary and the mushy layer [5].

5. Results and discussion

Numerical solutions of the system of ordinary differential equations were obtained by shooting on the fixed computational domain $0 \le \xi \le 1$, where $\xi = \eta/\mu$. We use these solutions to examine the effects of varying the density ratio r and the segregation coefficient k.

As r increases, both the linear growth rate of the mushy layer μ and the volume fraction of solid ϕ diminish (Figs. 6a and 6b). These are consequences of the same geometrical effect described in section 2. Although very good predictions of the growth rates of mushy layers have been obtained previously using models that ignored the change of density upon solidification [5,9], recent experiments by Shirtcliffe et al. [21], measuring the solid fraction in mushy layers, found less satisfactory agreement with the results of such models. However, it has been demonstrated by Chiareli and Worster [19] that excellent predictions of the solid fraction can be obtained once the effects of expansion are included in the analysis. The accurate prediction of the solid fraction within mushy layers is of profound importance in situations where natural, convective flow of the interstitial melt can occur; for example, when a less dense solute is rejected during solidification from below. In recent years, considerable attention has focused on the solutal convection within mushy layers formed from aqueous solutions of ammonium chloride. In a typical such experiment, with $\mathscr{S} = 5$, $\mathscr{C} = 20$ and $\theta_\infty = 1$, the solid fraction before convection begins is predicted to be $\phi_0 = 0.05$ at the base of the mushy layer if contraction is ignored. Our calculations give $\phi_0 = 0.03$ when $r = 1.5$, which is the appropriate value for this system. The difference
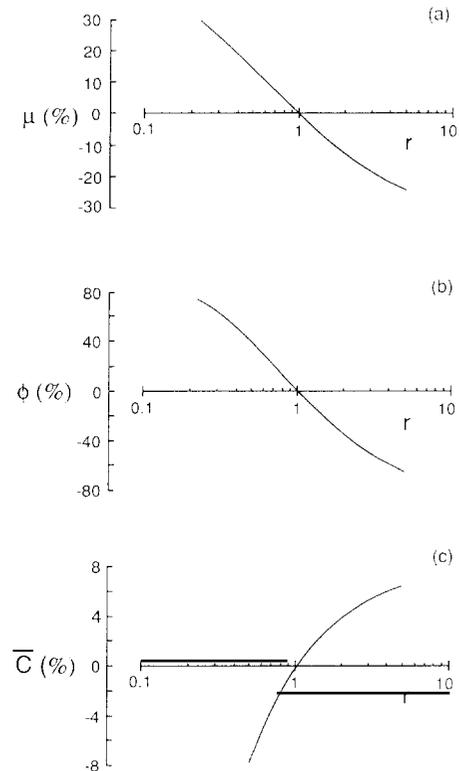

Fig. 6. Changes in (a) the growth rate, (b) the solid fraction, and (c) the bulk concentration at the bottom of the mushy layer as functions of the density ratio r, shown as percentages relative to the case $r = 1$ corresponding to no expansion. Parameter values used were $\mathscr{S} = \mathscr{C} = \theta_\infty = 1$, $k = 0$.

between these estimates of the solid fraction correspond to almost a factor of 2 in the estimate of the permeability of the layer, according to the Carman–Kozeny formula, which would lead to the same fractional difference in an estimate of the Rayleigh number driving convection.

The flow induced by contraction causes macro-segregation of the alloy, as shown in Fig. 6c. While small, such levels of segregation may yet be undesirable in the processing of materials, especially for the semi-conductor industry where high tolerances are required. Unlike segregation caused by buoyant convection, this cannot be avoided by forming materials in space and must be taken into account when analysing the feasibility of such enterprises.

Since the rate of diffusion of solute is slow compared with the rate of growth of a mushy layer, significant macro-segregation is only achieved by flow of the interstitial fluid. By contrast, micro-segregation on the scale of individual dendrites is determined by the local processes involved in maintaining the interior of the mushy layer near equilibrium. In particular, the segregation coefficient k plays a central role in determining how the solute is partitioned between the solid and the liquid fraction of the mushy layer. The similarity solution has the features that the liquid concentration depends only on η while the solid concentration is independent of η.

As solid grows within the mushy layer, solute is rejected into the interstices. For larger values of the segregation coefficient k, less solute is rejected and this allows a greater fraction of the mushy layer to be solid (Fig. 7). Variations in k do not, however, alter the thickness of the mushy layer much since there is little accumulation of rejected solute ahead of the mush–liquid interface. Note that the solid fraction tends to unity as $k \to 1 -$, as expected, but remains bounded away from unity throughout the mushy layer when $k < 1$. This is a consequence of the total neglect of diffusion within the solid phase.

6. Conclusions

We have determined a very general expression for the rate of advance of a planar solidification
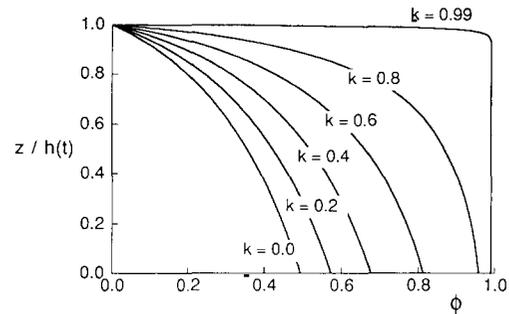

Fig. 7. The solid fraction ϕ in the mushy layer as a function of depth in the layer for different values of the segregation coefficient k. The mushy layer becomes almost all solid as k approaches 1. The dimensionless parameter values used to calculate these curves were $\mathscr{S} = \mathscr{C} = \theta_\infty = r = 1$.

front in a binary alloy that incorporates the change in density that occurs as liquid converts to solid and accounts for non-zero values of the segregation coefficient. By analysing this result in the limit $D/\kappa \to 0$, which is appropriate for most systems, we have been able to draw some important conclusions that can be expressed quite simply. Principal among these is that the solidification rate is controlled by the diffusion of solute away from the solid–liquid interface when the temperature of the cooled boundary is greater than the initial solidus temperature of the alloy. Once the boundary is colder than this, solutal diffusion is no longer rate controlling and the interface advances as if it were growing from a pure melt of freezing temperature equal to the solidus temperature.

The composition C_s of the solid that forms can be estimated simply as follows. In the regime limited by solutal diffusion $C_s \approx kC_B$, where C_B is the concentration on the liquidus corresponding to the temperature T_B of the cold base and k is the segregation coefficient. Once solutal control is lost, $C_s \approx kC_0$, where C_0 is the initial concentration of the melt.

Our results indicate that, except when the initial concentration is small, as expressed by

$$(1 - k)C_0 = O\left[(D/\kappa)^{1/2}\right],$$

the liquid becomes supercooled whenever

$$T_B < T_L(C_0) - (D/\kappa)^{1/2}[T_\infty - T_L(C_0)].$$

Since D/κ is typically very small, constitutional supercooling is clearly a common occurence. It is alleviated by the formation of a mushy layer.

The difference in density between solid and liquid drives a non-solenoidal flow of the interstitial fluid within the mushy layer, even when no external forces are acting. There are two significant consequences of the transport of solute by such a flow. One is that the porosity, and hence the permeability, of the layer is altered, which has important implications for the onset of natural convection within the interstices, for example. The other is that it causes macro-segregation of the alloy that cannot be eliminated by forming the solid in microgravity, since it is intrinsic to the solidification itself.

7. Acknowledgements

8. References

[1] H.S. Carslaw and J.C. Jaeger, Conduction of Heat in Solids (Oxford University Press, Oxford, 1959).

[2] L. Rubinstein, The Stefan Problem, Translation of Mathematical Monographs, Vol. 27 (Am. Math. Society, Providence, RI, 1971).

[3] M.G. Worster, The dynamics of mushy layers, in: Interactive Dynamics of Convection and Solidification, NATO ASI Series E219, Eds. S.H. Davis, H.E. Huppert, U. Müller and M.G. Worster (Kluwer, Dordrecht, 1992) pp. 113–118.

[4] H.E. Huppert, J. Fluid Mech. 212 (1990) 209.

[5] M.G. Worster, J. Fluid Mech. 167 (1986) 481.

[6] M.C. Schneider and C. Beckermann, in: Interactive Dynamics of Convection and Solidification, NATO ASI Series E219, Eds. S.H. Davis, H.E. Huppert, U. Müller and M.G. Worster (Kluwer, Dordrecht, 1992) pp. 195–197.

[7] A.R. Umantsev, Sov. Phys.-Cryst. 30 (1985) 87.

[8] J.N. Dewynne, S.D. Howison, J.R. Ockendon and W. Xie, J. Austral. Math. Soc. B 31 (1989) 81.

[9] H.E. Huppert and M.G. Worster, Nature 314 (1985) 703.

[10] V. Alexiades and A.D. Solomon, Mathematical Modeling of Melting and Freezing Processes (Hemisphere, Washington, DC, 1993).

[11] J.W. Rutter and B. Chalmers, Can. J. Phys. 31 (1953) 15.

[12] R.F. Sekerka, Morphological stability, in: Crystal Growth: An Introduction, Ed. P. Hartman (North-Holland, Amsterdam, 1973) pp. 403–442.

[13] W.W. Mullins and R.F. Sekerka, J. Appl. Phys. 35 (1964) 444.

[14] S.H. Davis, J. Fluid Mech. 212 (1990) 241.

[15] R.N. Hills, D.E. Loper and P.H. Roberts, Quart. J. Appl. Math. 36 (1983) 505.

[16] A.C. Fowler, IMA J. Appl. Math. 35 (1985) 159.

[17] M.J. Beran, Statistical Continuum Theories (Interscience, New York, 1968).

[18] R.C. Kerr, A.W. Woods, M.G. Worster and H.E. Huppert, J. Fluid Mech. 216 (1990) 323.

[19] A.O.P. Chiareli and M.G. Worster, J. Crystal Growth 125 (1992) 487.

[20] V.V. Vas'kin, Izv. Akad. Nauk SSSR, Metally 1 (1986) 83 (published by Allerton Press).

[21] T.G.L. Shirtcliffe, H.E. Huppert and M.G. Worster, J. Crystal Growth 113 (1991) 566.